TOWARDS INCREASED INDUSTRIAL APPLICATION OF ROTOR AEROELASTIC CFD

Markus Dietz, Eurocopter Deutschland GmbH, 81663 München, Germany
Oliver Dieterich, Eurocopter Deutschland GmbH, 81663 München, Germany

Abstract

The present paper describes recent developments in the application of aeroelastic rotor CFD at Eurocopter. The aeromechanic tool environment is presented and applied to an isolated rotor in forward flight. A weak coupling methodology between CFD and comprehensive rotor codes is applied in order to trim the rotor towards prescribed trim objectives and thus to allow for a meaningful comparison of the computational results to flight test data. The block-structured CFD code FLOWer (DLR) is used for the aerodynamic simulation. The flight mechanics and rotor dynamics simulation is carried out using a Eurocopter in-house rotor code and the comprehensive code CAMRAD II. The weak coupling interface between FLOWer and CAMRAD II has been recently developed and will thus be described in more detail. The coupled computational results are compared to flight test data. The comparison is carried out with respect to rotor performance and blade loads. Finally an outlook will be given on the planned future extension of the coupling interface for complete helicopter simulation and trim.

1. NOMENCLATURE

1.1. Symbols

θ_0	collective pitch angle [°]
θ_C	lateral cyclic pitch [°]
θ_S	longitudinal cyclic pitch [°]
ψ	Azimuth angle
C_T	thrust coefficient
C_{Mx}	rotor mast roll moment coefficient
C_{My}	rotor mast pitch moment coefficient
C_nMa^2	sectional normal force coefficient
C_mMa^2	sectional pitching moment coef.
C_pMa^2	Mach-scaled pressure coefficient
$C_{Fz}Ma^2$	sectional thrust coefficient (in z-direction of rotating system)

1.2. Coordinate Systems

Rotating rotor hub system:
- x-axis in radial direction from root to tip
- y-axis in tip path plane from trailing edge to leading edge
- z-axis in rotor hub direction

Non-rotating rotor hub system:
- x-axis longitudinal pointing backwards
- y-axis lateral pointing to starboard
- z-axis in rotor hub direction

1.3. Trim Numbering

- The initial trim of the comprehensive code is denoted as 0^{th} trim.
- The FLOWer calculation following the n^{th} comprehensive code trim is denoted as n^{th} FLOWer trim.

1.4. Acronyms

ADT	Alternating Digital Tree
ALE	Arbitrary Lagrangian Eulerian
BEM	Blade Element Model
CAMRAD II	Comprehensive Analytical Model of Rotorcraft Aerodynamics and Dynamics
CFD	Computational Fluid Dynamics
CHANCE	Complete Helicopter Advanced Computational Environment
CSD	Computational Structural Dynamics
DFT	Discrete Fourier Transformation
DLR	Deutsches Zentrum für Luft- und Raumfahrt e.V.
DOF	Degree Of Freedom
ECD	Eurocopter Deutschland GmbH
GCL	Geometric Conservation Law
GUI	Graphical User Interface
IAG	Institut für Aerodynamik und Gasdynamik
SHANEL	Simulation of Helicopter Aerodynamics, Noise and Elasticity

2. INTRODUCTION

The accurate prediction and reproduction of rotor aerodynamic and aeroelastic behaviour plays an important role in rotor design and rotor assessment. While from an aerodynamic point of view the main focus is on rotor performance and blade loads, vibratory blade and hub loads and dynamic stability

are the particular interests of rotor dynamics. The increasing requirements with respect to prediction accuracy bring these disciplines closer together aiming on the development and application of highly sophisticated tool chains. The simulation of these problems are usually carried out using so called comprehensive codes including aerodynamic and dynamic rotor models in combination with a flight mechanics functionality providing the rotor and/or rotorcraft trim state. In this context the focus of this paper is put on aerodynamic, performance and blade load aspects.

Within the last years extensive activities have been initiated in order to extend the aerodynamic and structural modules towards high-fidelity methods with significantly increased accuracy. In the German-French project SHANEL [1] a cooperation between Eurocopter, DLR and ONERA has been established in order to further develop advanced simulation methods towards the trimmed aeroelastic simulation of main rotor systems and complete rotorcrafts. On aerodynamic side the focus is put on the replacement of simple blade element models (BEM) by CFD aerodynamics, while the blade structural dynamics model is extended from a modal approach towards finite element beam models or even more advanced general CSD modelling. As an intermediate step in this framework Eurocopter has introduced the weak coupling methodology between the CFD code FLOWer (DLR) [2] and comprehensive rotor codes. The existing weak coupling interface to an in-house rotor code was further extended between the FLOWer code and the commercial comprehensive rotor code CAMRAD II [3] representing state-of-the-art.

The intention of this paper is the assessment of different aerodynamic and structural dynamic models by cross-comparison and also by checking with flight tests: Focus is mainly given on the aerodynamic models which will include standard BEM aerodynamics in combination with free-wake models on the one hand and the weak coupling with the CFD code FLOWer on the other hand. The structural modelling of the rotor is based on either a modal approach or on beam finite elements both representing industrial modelling approaches of today. The computational methods are applied to an experimental main rotor in cruise forward flight condition at 135kts which is a typical rotor design point. The different numerical results will be compared with flight test data obtained from a BK117 measurement campaign. The comparison is carried out with respect to rotor performance and blade loads.

Future developments target on the extension of the current isolated rotor coupling and trim capabilities towards the trimmed CFD simulation of the complete helicopter. The related activities are performed in close cooperation with IAG [1]. First steps in this direction are currently carried out and will be briefly described in this paper: A CFD grid system of the complete EC145 helicopter was prepared and the fuselage blocking effect on the rotor flow was studied. First results will be presented in the final chapter of the paper.

3. COMPUTATIONAL METHODS

3.1. FLOWer

The aerodynamic computations were performed using the block-structured CFD solver FLOWer developed by DLR [2]. FLOWer was compiled in the framework of the MEGAFLOW project [4] and is available at ECD through the cooperation with DLR in the framework in CHANCE [5] and SHANEL projects.
FLOWer solves the three-dimensional, compressible and unsteady Navier-Stokes equations. The equations are formulated in a non-inertial rotating reference system with explicit contributions of centrifugal and Coriolis forces to the momentum and energy equations. Furthermore FLOWer includes the ALE-Formulation which facilitates the computation of deforming meshes by adding whirl-fluxes resulting from the cell face motion to the convective flux portion. The Geometric Conservation Law (GCL) evaluates the cell volumes of the deformable mesh consistent to the cell face velocities. This ensures the preservation of uniform flow on deformable grids.
The discretization of space and time is separated by the method of lines. FLOWer includes a cell-vertex and a cell-centred formulation. Convective fluxes are computed using the JST scheme [6] which uses 2^{nd} order central differences with artificial dissipation for stabilization. The integration in pseudo time is carried out using a 5-stage hybrid Runge-Kutta method. In order to circumvent the time step limitation of the explicit scheme FLOWer makes use of the dual time stepping technique with a second order implicit time integration operator in case of unsteady flow [7].
FLOWer features the Chimera-technique allowing for arbitrary relative motion of aerodynamic bodies [8]. Relative motion of grids can be arbitrarily defined via the input file by setting up the required kinematic chain of coordinate systems. Chimera connectivities are determined using hole cutting and interpolation. The ADT search method is applied in order to identify donor cells in curvilinear grids.
Within the past years additional helicopter specific features have been integrated into FLOWer mainly by IAG [9]. This includes interfaces for strong (i.e. time-accurate) and weak coupling, a multi-block blade grid deformation tool and rotor specific post-processing. The weak coupling interface to CAMRAD II has been integrated at ECD and will be described in more detail in the present paper.

3.2. CAMRAD II

CAMRAD II is a commercial aeroelastic analysis code for helicopters and rotorcrafts that incorporates a combination of state-of-the-art technologies like multibody dynamics, nonlinear finite elements, structural dynamics and rotorcraft aerodynamics [3].
The aerodynamic modelling of rotor systems in CAMRAD II is based on lifting line theory assuming that the rotor blade has a high aspect ratio, or more generally that spanwise variations of the aerodynamic environment are small. This assumption allows the problem to be split into separate blade wing and rotor wake models, which are solved individually and combined. Two-dimensional, steady airfoil data are extracted from airfoil tables for solving the wing problem. Code-internally the coefficients are corrected for Mach and Reynolds effects, yawed flow and unsteady behaviour (Dynamic Stall modelling). Regarding the wake problem the induced velocity distribution on the rotor disk is either derived by analytical downwash models or computed by prescribed or Free-Wake methods [10].
For all structural dynamic elements of CAMRAD II, the rigid body motions can be large due to multibody dynamics, and the kinematics of the interfaces and rigid body motion are always exact. For the finite beam elements [11], the elastic motion is represented in addition by the deflection, extension, and torsion of the beam axis. The beam element implemented in CAMRAD II offers three different geometric models ranging from exact kinematics of the beam elastic motion to retaining only second-order effects of elastic motion in the strain energy and kinetic energy, restricting the elastic motion to moderate deflection. The beam element features in addition two structural models. The first structural model is beam theory for anisotropic or composite materials, the second structural model is based on Euler-Bernoulli beam theory for isotropic materials with an elastic axis, the undistorted elastic axis straight within the component. For the numerical models used in this paper, the second option was applied.
Further information on the isolated rotor model used for the present investigations will be provided in section 5.3.

3.3. In-House Rotor Code

Eurocopter's in-house rotorcraft comprehensive code is mainly used for flight mechanics and enables the study of single helicopter components like isolated rotors as well as complete configurations with related substructures.
As it is the case for CAMRAD II, it trims the rotor based on a lifting-line method with 2D airfoil tables.
The elastic blade model considers the blade as a quasi one-dimensional Euler-Bernoulli beam. It allows for deflections in flap and lag direction and elastic torsion along the blade axis. In addition to the assumption of a linear material law, tension elongation and shear deformation are neglected. However, possible offsets between the local cross-sectional centre of gravity, tension centre and shear centre are accounted for, thus coupling bending and torsional DOFs.
The blade model is based on a geometrically nonlinear formulation, connecting rigid segments through virtual joints. At each joint, elastic rotations are permitted about the lag, flap and torsion axes. Since the use of these rotations as degrees of freedom (DOFs) would yield a rather large system of equations, the number of equations is reduced by a modal Rayleigh-Ritz approach. A limited set of mode shapes together with their weighting factors are used to yield a deformation description. Therefore, any degree of freedom can be expressed as

$$h(r,\psi) = \sum_{i=1}^{n} q_i(\psi) \cdot \hat{h}_i(r) \qquad (1)$$

where n is the number of modes, q_i the generalized coordinate of mode i (a function of the azimuth angle ψ), and $\hat{h}_i$ is the mode shape (a function of the radial position r). It is obtained by an eigenvalue analysis of the beam in vacuum, resulting in coupled flap/lag mode shapes and decoupled torsion modes.

4. CODE COUPLING

4.1. Coupling Methodology

Coupling between comprehensive codes and CFD is performed for the following three main purposes:

- Replacing the simple comprehensive code aerodynamic model with the more sophisticated CFD aerodynamics.
- Consideration of the blade articulation and deformation in the CFD computation.
- Provision of a trimmed flight state.

The first two issues are closely linked to each other. A consistent coupled aerodynamic/dynamic method needs to reproduce the coupled physics of the aeromechanic problem, i.e. the aerodynamic loads must match with the blade dynamic response evoked by them.
This requirement is fulfilled both in case of time-accurate (strong) coupling method and in case of the (converged) weak coupling method. The major drawback of strong coupling is the fact that a trim state is not directly provided [12]. One obtains a coupled solution for a given set of control angles, resulting in a set of mean rotor loads. In order to obtain a prescribed trim (a prescribed set of mean rotor loads) the coupled computation has to be iteratively restarted with modified controls until the objective is met. Furthermore the transient aeroelastic response is modelled, hampering the convergence towards a periodic solution.

The main advantage of the weak coupling method is the inherent trim possibility [13][14]. A trimmed flight state is inevitable in order to allow for a meaningful comparison to flight test data, e.g. in terms of rotor performance and blade loads. The weak coupling method used in the present paper is realized basically in the same way for both the coupling between the in-house rotor code and FLOWer and CAMRAD II and FLOWer: The comprehensive code uses CFD loads to correct its internal 2D aerodynamics and re-trims the rotor. The blade dynamic response is introduced into the CFD calculation in order to obtain updated aerodynamic loads. This cycle is repeated until the CFD loads match with the blade dynamic response evoked by them. A criterion for this converged state is given by the change in the free controls with respect to the preceding cycle. Convergence has been reached after the changes in the controls have fallen below this imposed limit.

The individual steps of the coupling scheme can be summarized as follows [13][14]:

1. The comprehensive code determines an initial trim of the rotor based on its internal 2D aerodynamics derived from airfoil tables. The blade dynamic response is stored.
2. The blade dynamic response is taken into account in the subsequent CFD calculation by applying the corresponding articulation and deformation to the blade surface and by performing the related deformation of the surrounding volume mesh.
3. The CFD calculation determines the 3D blade loads in the rotating rotor hub system for every azimuth angle and radial section of the blade.
4. For the next trim the comprehensive code uses a load given by

$$\overline{F}_{eff}^{\,n} = \overline{F}_{2D}^{\,n} + \overline{F}_{3D}^{\,n-1} - \overline{F}_{2D}^{\,n-1} \tag{2}$$

   F_{2D}^{n} represents the free parameter for the actual trim. A new dynamic blade response is obtained.
5. Steps (2) to (4) are repeated until convergence has been reached, i.e. when the difference

$$\Delta\overline{F}_{2D}^{\,n} = \overline{F}_{2D}^{\,n} - \overline{F}_{2D}^{\,n-1} \rightarrow 0 \tag{3}$$

   tends to zero and the trim-loads depend only on the 3D CFD aerodynamics in case of full convergence.

The scheme, as described above, requires the separate storage of the lifting line portion of the comprehensive code aerodynamics as it is required for the next trim (see equation 2). In order to avoid this procedure one can modify the formulation as follows [15]:

The actual loading used for trim at iteration n is given by equation (2):

$$\overline{F}_{eff}^{\,n} = \overline{F}_{2D}^{\,n} + \Delta\overline{F}^{\,n} = \overline{F}_{2D}^{\,n} + \overline{F}_{3D}^{\,n-1} - \overline{F}_{2D}^{\,n-1} \tag{4}$$

The loading of the previous iteration n-1 is given by

$$\overline{F}_{eff}^{\,n-1} = \overline{F}_{2D}^{\,n-1} + \Delta\overline{F}^{\,n-1} = \overline{F}_{2D}^{\,n-1} + \overline{F}_{3D}^{\,n-2} - \overline{F}_{2D}^{\,n-2} \tag{5}$$

From equation (5) one obtains

$$\overline{F}_{2D}^{\,n-1} = \overline{F}_{eff}^{\,n-1} - \Delta\overline{F}^{\,n-1} = \overline{F}_{eff}^{\,n-1} - (\overline{F}_{3D}^{\,n-2} - \overline{F}_{2D}^{\,n-2}) \tag{6}$$

By inserting (5) in (3) one obtains

$$\begin{aligned} \Delta\overline{F}^{\,n} &= \overline{F}_{3D}^{\,n-1} - \overline{F}_{2D}^{\,n-1} = \overline{F}_{3D}^{\,n-1} - \overline{F}_{eff}^{\,n-1} + \Delta\overline{F}^{\,n-1} \\ \Delta\overline{F}^{\,n} &= \Delta\overline{F}^{\,n-1} + (\overline{F}_{3D}^{\,n-1} - \overline{F}_{eff}^{\,n-1}) \end{aligned} \tag{7}$$

Consequently the update of the current 2D lifting line portion can be obtained from the previous update (correction of the lifting line portion of the previous iteration) by adding the difference of the CFD loads and the total trim loads of the previous iteration. No separate storage of the lifting line portion is required.

4.2. Coupling Implementation between the In-House Rotor Code and FLOWer

The coupling implementation between the in-house rotor code and FLOWer is explained in detail in Reference [16]. The basic characteristics of the implementation are repeated in the following.

The coupling scheme makes use of the first formulation provided in the previous section, i.e. the lifting line aerodynamics is separately stored. The loads vector F usually includes three load components in the rotating rotor hub frame, namely the sectional thrust F_z, the sectional in-plane drag F_y and the sectional blade pitching moment M_x around the local airfoil quarter chord location. Loads are evaluated at each spanwise station of the CFD mesh and stored as line loads, i.e. forces are stored in [N/m] and the pitching moment is stored in [Nm/m].
Before providing the CFD loads to the comprehensive code an auxiliary tool reads in the loads of each rotor blade and combines the loads of the last quarter revolution (for a four-bladed rotor) of each rotor blade to the loading of one complete rotor revolution. This step makes it possible to use the latest (i.e. best periodically converged) portion of the flow solution.
The comprehensive code reads in the CFD line loads and re-transforms them to discrete loads to be applied at the rigid body blade elements by piecewise integration. In order to apply the loading for the re-trim the comprehensive code performs a Fourier analysis considering a user-defined number of harmonics.
The reconstruction of the articulated and deformed blade surface in FLOWer is based on the modal description: The blade axis and the blade torsion

distribution for a given azimuth angle is composed from the superposition of the mode shapes, each of which is weighted by the corresponding generalized coordinate according to equation (1). The variation of the generalized coordinate of each mode versus azimuth is described in the frequency domain using Fourier coefficients up to a certain harmonic.
The reconstruction process is based on the radial discretization of the comprehensive code blade model. Displacement and rotation data for each CFD spanwise blade section are obtained by linear interpolation from the comprehensive code blade discretization and the reference blade surface is deformed accordingly.

The above description of the coupling implementtation shows that no constraints concerning an adaptation of the spanwise blade discretizations need to be taken into account: Arbitrary blade discretizations on either side are made possible by the exchange of line loads and by an interpolation of blade deformation data.
On the one hand this is an advantage as the blade discretizations on either side can be set up completely independently from each other, only driven by the requirements of the corresponding code. But on the other side recent results have shown that the line loads exchange introduces a load conservativity error into the coupling scheme, i.e. both the integral blade loads and load distribution are not necessarily exactly conserved during the exchange process. This is due to the fact that a piecewise integration of the line loading is carried out using modified integration limits.
While the relative error is very small for the integral rotor thrust it can become larger for the rotor torque (and hence the rotor power required). As a remedy some adaptation of the comprehensive code blade discretization to the CFD discretization can be performed, i.e. the blade discretization can be refined in regions of strong gradients in the spanwise CFD load distribution.

4.3. Coupling Implementation between CAMRAD II and FLOWer

The weak coupling interface between FLOWer and CAMRAD II has been newly developed at ECD in the framework of the SHANEL-L project. The basic weak coupling functionality is already included in CAMRAD II. In order to perform coupling to FLOWer additional interfacing tools and a Python-based script environment were set up. FLOWer was modified in order to allow for the consideration of CAMRAD II blade deformation data, while CAMRAD II access to CFD load data was conventionally established using external files.

The coupling scheme between FLOWer and CAMRAD II utilizes the second formulation provided in section 4.1. This means, the lifting line portion of the aerodynamics is not separately stored. Instead the load update is formulated based on the previous load update and the total trim loads of the last iteration according to equation (7). We decided to put emphasis on a strictly conservative coupling implementation, both concerning loads and deformation exchange. As a consequence we forgo the independency of blade discretizations and request instead an adapted discretization between FLOWer and CAMRAD II. The details of the coupling implementation will be described in the following. A flow chart of the coupling process is shown in Figure 1.

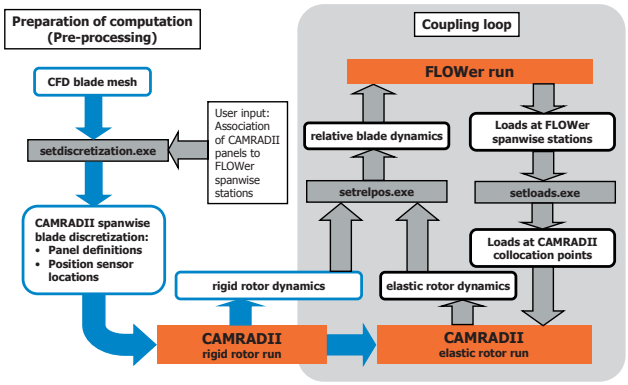

Figure 1: Flow chart of the coupling between FLOWer and CAMRAD II

Reconstruction of the blade surface

In order to prescribe the blade dynamic state at the CFD spanwise blade stations the CAMRAD II position sensor functionality is applied: CAMRAD II allows for the specification of arbitrary radial locations for position sensor output. The sensor output includes the *absolute* location of the blade quarter chord location in the rotating blade frame and the three Euler rotation angles of the blade section relative to the reference blade. Note that the computation of position sensor data in CAMRAD II is consistent to the multibody approach and the finite beam element representation of the blade. Exploiting the shape functions of the beam elements, no accuracy is lost if the position sensor locations do not match the beam element boundaries.
The information required by the CFD method is however the *relative* position of the sectional quarter chord location, i.e. the location relative to the original location of the undeformed reference blade. As CAMRAD II is based on multibody dynamics only absolute location data are provided and direct output of displacement information is not supported. In order to provide the required displacement data a rigid rotor CAMRAD II run is performed as a preprocessing step. The relative displacement information is then computed from the difference of the absolute position sensor locations of the actual trim

computation and the absolute position sensor locations of the rigid rotor pre-run. This task is applied by a pre-processor tool in the frame of the script-controlled coupling loop. The final displacement and rotation information is provided to FLOWer as Fourier coefficients versus azimuth and the actual azimuth angle dependent deformation data are obtained from inverse Fourier transformation.

Load transfer

As previously mentioned the transfer of loads is supposed to be performed in a conservative manner. As a consequence an adapted spanwise blade discretization has to be required. In this context "adapted discretization" does not mean that FLOWer and CAMRAD II need to use exactly the same number of spanwise elements at the same spanwise locations along the coupled spanwise range. The spanwise discretization of the CFD mesh is usually higher than the number of spanwise aerodynamic blade elements in CAMRAD II. An increase of the spanwise elements in CAMRAD II (usually <30) towards the range of grid cells used in CFD (usually ~100) would lead to numerical issues.
For this reason the current implementation allows for a multigrid-like approach: The CAMRAD II aerodynamic panelization is a subset of the CFD grid, resulting from a coarsening of the spanwise CFD discretization. It is automatically generated from the CFD blade mesh using a user-provided association table. One CAMRAD II aerodynamic panel matches one or a sequence of subsequent spanwise CFD blade elements. The *discrete* loads of this sequence of CFD spanwise elements can be directly added up in order to obtain the discrete loading of the associated CAMRAD II panel. We include all six load components (three forces and three moments) in the load exchange procedure. While the discrete force components can be directly summed up over all contributing CFD elements, the resulting moment components are the sum of the free moments of the contributing CFD elements plus the portion resulting from the CFD element forces acting around the CAMRAD II aerodynamic panel moment reference point. This point is located at the quarter chord location at the radial CAMRAD II panel center. In order to obtain a definite reference for its coordinates in deformed state additional position sensors are defined at the load collocation points as described in the previous section.
In order to avoid interpolation errors a consistent azimuthal discretization of the load data with respect to the internal azimuthal resolution of CAMRAD II is preferred. While the azimuthal resolution of the CFD solver is usually close to 1° it is much coarser on CAMRAD II side, normally around 15°. As a consequence one has to provide a procedure in order to transfer the loading to the new azimuth interval. Simple linear interpolation between the adjacent azimuth locations of the CFD computation is not appropriate. Instead one has to guarantee that the full harmonic excitation of the CFD loading which is resolvable with the CAMRAD II resolution is transferred. For this purpose a Discrete Fourier Transformation of the loads versus azimuth is performed. The number of meaningful harmonics is limited by the number of azimuth steps on CAMRAD II side applying the Nyquist criterion. The discrete values at the CAMRAD II azimuth stations are then obtained by inverse Fourier transformation.

As already explained for the blade deformation part all load preparation work is performed by a pre-processor tool embedded into the script-controlled coupling loop. Summing up the following tasks are performed by the load pre-processing tool:

- Read in the blade load files from FLOWer and reconstruct one complete rotor revolution from the last quarter revolution of each blade.
- Transfer the loading from CFD to CAMRAD II spanwise discretization.
- Transfer the loading from CFD to CAMRAD II azimuthal discretization using DFT and inverse Fourier transformation.

4.4. Script environment

The complete coupling procedure is controlled by a Python script. The script performs the sequential calls of FLOWer and the comprehensive codes as well as all intermediate data preparation tasks. In order to ease the setup of the coupled computation a Graphical User Interface has been set up. The graphical front end is shown in Figure 2.

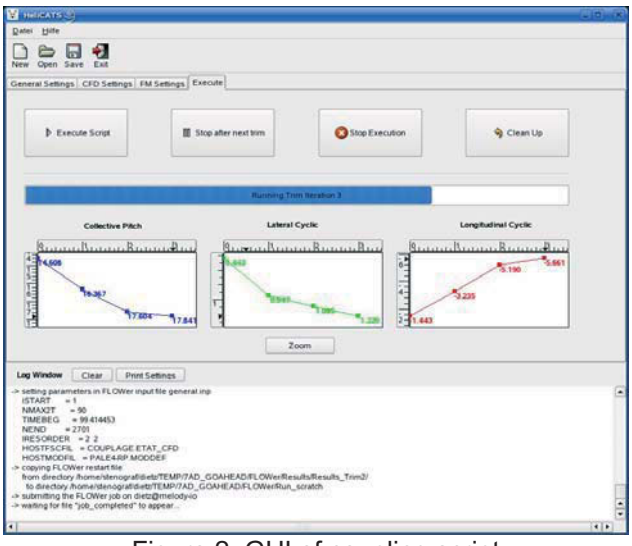

Figure 2: GUI of coupling script

Besides the simplified preparation of the coupled run the GUI allows for online visualization of the trim convergence, adaptation of parameters during runtime (e.g. the number of time steps of the CFD runs) and automatic convergence detection.

5. TEST CASE DEFINITION

5.1. Flight Condition and Flight Test Data

The test case chosen for the coupled computations is a four-bladed experimental hingeless rotor – featuring a Boelkow rotor hub and exchangeable blade tips – in steady forward flight condition at 135kts. Flight test data are available from test campaigns on the BK117 helicopter. The experimental test bed is shown in Figure 3.

The computational model is restricted to the isolated rotor. Hence the trim objective for the isolated rotor has to be derived. We trim the rotor for thrust and rotor pitch and roll moment. Collective and cyclic pitch are used as free control inputs while the rotor shaft pitch and roll attitude is prescribed from flight test data and held fixed during the coupling process.
Rotor pitch and roll moment were measured during flight test and can thus directly be used for trimming. The rotor thrust is not available from flight test. In order to provide a realistic value a complete helicopter trim computation has been performed with an in-house flight mechanics code. Rotor thrust and hub moments were extracted from the trim result. The computed rotor hub moments turned out to be in very good agreement to the measured flight test values, supporting the reliability of the computed rotor thrust.

Figure 3: BK117 experimental test bed
(© Eurocopter Deutschland GmbH)

The rotor flight condition and trim objectives are summarized in Table 1.

True Air Speed	135 kts
Rotor advance ratio	0.31
Flight speed Mach number	0.206
Blade tip Mach number	0.661
Blade tip Reynolds number	1.32×10^7 /m
Rotor shaft pitch angle	-6.0°
Rotor shaft roll angle	+0.2°
Far field pressure	84100 Pa
Far field temperature	7,7°C
Thrust coefficient (derived from flight mechanics computation)	0.0071
Rotor hub pitch moment coefficient (from flight test)	8.52×10^{-5}
Rotor hub roll moment coefficient (from flight test)	7.48×10^{-6}

Table 1: Flight condition and trim objective

Note that the blade features two characteristics which need to be particularly considered in the dynamic and aerodynamic modelling.
First the blade is equipped with two pairs of trailing edge tabs one of which is deflected significantly upwards. While the tab modeling is a quite forward procedure for BEM approaches, it significantly impacts the structured blade mesh generation for the CFD solver. More details will be provided in section 5.2.
Second the blade features pendulum absorbers in order to reduce the vibratory hub loads. The pendulum absorbers are of special interest for the dynamic blade model in order to increase the accuracy of the blade dynamics prediction. Further information will be given in section 5.3.

Comparison of computational results to flight test data will be carried out with respect to rotor performance (power required) and blade loads.
Concerning performance comparison the total engine power is available from flight test. It is measured via the engine torque at the drive shafts between the engines and the main gear box. Hence the measured power includes main gear box losses, tail rotor power and auxiliary device power. The net main rotor power required is estimated using a computational value for the tail rotor power and empirical values for auxiliary devices power and gear box losses.
The dynamic instrumentation of the blade includes flap bending moment sensors, lag bending moment sensors and torsion moment sensors. The sensors of interest are installed at the following locations:

Flap bending:

- MB522: r = 522 mm , r/R = 0.095
- MB2310: r = 2310mm, r/R = 0.42
- MB3410: r = 3410 mm, r/R = 0.62
- MB4510: r = 4510 mm, r/R = 0.82

Lag bending:

- MZ1210: r = 1210 mm , r/R = 0.22

Blade torsion:

- MT1290: r = 1290mm, r/R = 0.235

5.2. CFD Setup

The CFD computations have been carried out using the Chimera grid system depicted in Figure 4. The rotor blade includes the aerodynamic part of the blade and the portion of the blade neck from the most inboard profiled section down to the elliptical cross section connecting the blade to the rotor head. The rotor head is not modelled. The blade meshes use a multi-block topology with C-type topology in chordwise direction and O-type topology in spanwise direction. During the coupled computation the blade grids are deformed according to the current dynamic state of the blade using the multi-block grid deformation tool incorporated into FLOWer.
As previously mentioned the rotor blades feature two pairs of trailing edge tabs. In order to correctly capture the tab effect on the airfoil pitching moment and the related torsional response of the blade the tabs need to be included in the CFD model. The tabs represent an extension of the effective chord length, leading to an abrupt jump in the trailing edge contour at the spanwise tab boundaries. For coupling purposes FLOWer code-internally reconstructs a i-j-sorted surface description of the complete rotor blade from the wall patches of the different blocks contributing to the blade surface. Hence an adapted blocking in order to account for the chord size jump is not possible. Instead, the grid lines have to be bended around the kink in the surface contour, leading to a deteriorated mesh quality at the tab boundaries. This aspect is illustrated in Figure 5.

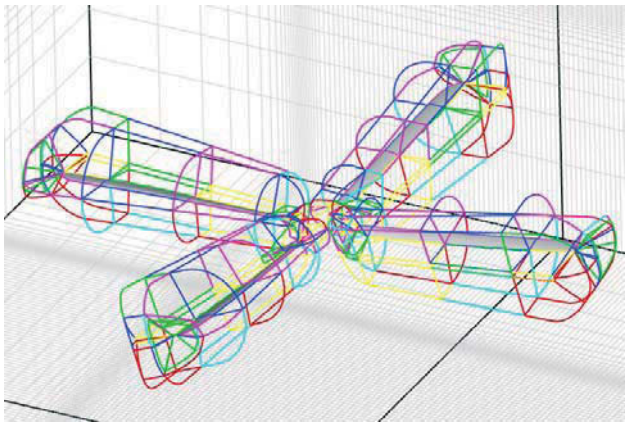

Figure 4: CFD Chimera grid system

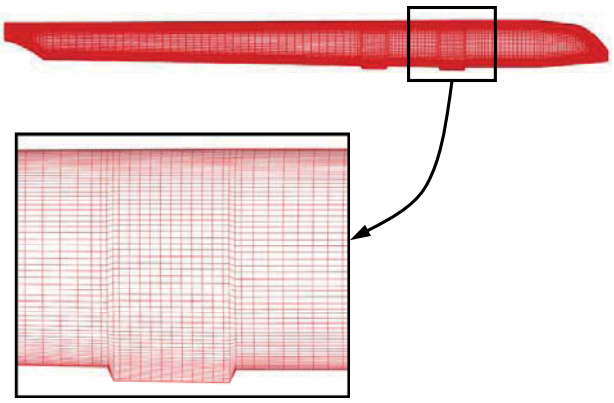

Figure 5: CFD blade surface including trailing edge tabs

The blade meshes are embedded into a Cartesian background grid. Cylindrical holes wrapping the blades are defined in order to blank grid cells in the background grid. At each physical time step of the computation the orientation of the cylindrical hole is adapted to the actual location of the articulated and deformed blade in the rotating hub system.

The grid data of the Chimera system are summarized in Table 2. The complete grid system consists of roughly 8 million grid cells.

Grid	Number of blocks	Number of cells
Blade grid	4 x 30	1,750,016
Background grid	4	1,327,104
Total	124	8,327,168

Table 2: CFD grid data

The kw-Wilcox turbulence model was chosen for the closure of the RANS equations and an azimuthal resolution of 1° per time step was used for all computations.
The computations were carried out on a local Linux cluster. On 24 CPUs a performance of about 40h wall clock per rotor revolution was obtained.

5.3. CAMRAD II Modeling

The CAMRAD II structural dynamic model of the rotor consists of 15 beam elements per blade featuring a high density of elements in the rotor hub and the blade neck area in order to account for large stiffness variations. Regarding kinematics a second order approximation proved to be sufficient in terms of accuracy mainly due to the number of elements and the moderate deflections observed in the investigated cases. Two degrees of freedom per beam element were enabled for flap bending and lag bending, torsion and elongation.
Control flexibility was taken into account assigning soft spring elements to the blade pitch control chain.

The flap absorbers attached to the blade necks were adequately modelled by a rigid body approach using joints, levers and inertia properties. Finally order reduction was performed selecting nine fully coupled dynamic modes per blade for the solution process.
Regarding the aerodynamic model, 29 panels were assigned to the rotor model in radial direction as shown in Figure 6. The panels were aligned to the end sections of the beam elements for consistent edges where appropriate. It should be noted that the number of panels is quite high in this model in order to ease the link to the CFD discretization of the blade.

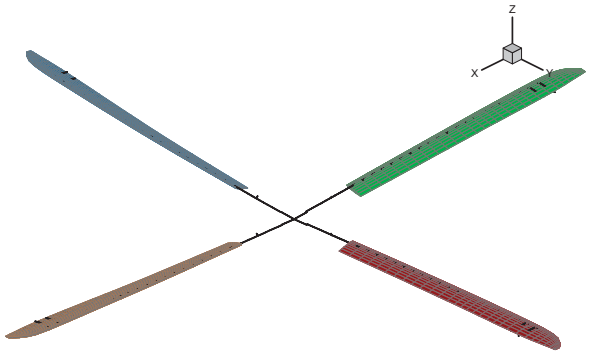

Figure 6: Rotor model presenting rotor code aerodynamic discretization

In case of coupling to CFD, the default uniform inflow model is engaged in order to provide aerodynamic damping to the solution process for low computational efforts. For comparison with CFD, different free wake models were investigated ranging from tip vortices fully rolled-up to multiple trailer wake models. Regarding the characteristics of the different wake models , see also Reference [17]. For all the wake models, default values for the parameter settings were used and no special tuning was performed representing an industrial approach aiming on predictive purposes.

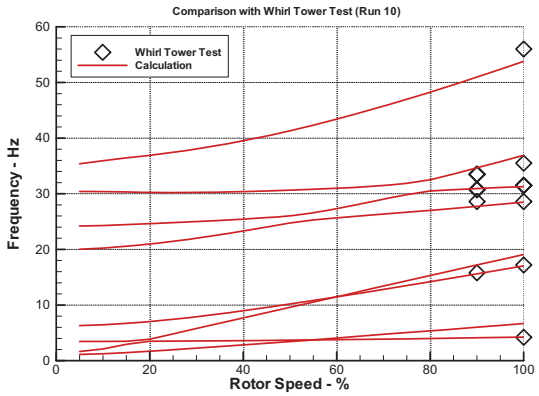

Figure 7: Comparison of model with whirl tower tests

The dynamic behaviour of the rotor model is demonstrated in the fan diagram in Figure 7. Acceptable agreement is noted for the frequencies with respect to experimental data measured on a whirl tower.

5.4. In-House Rotor Code Modeling

The dynamic model consists of 93 rigid elements. The first eight decoupled blade modes have been included into the mode-like deformation base. This includes the 1st lag mode, 1st and 2nd flap mode, 2nd lag mode, 1st torsion mode, 3rd flap mode, 3rd lag mode and 2nd torsion mode. The pendulum absorbers are not included in the dynamic model.
The code uses 45 azimuth stations per rotor revolution. The harmonic content of the blade dynamics is considered up to 5/rev. For re-trim purposes the code accounts for the CFD load variation up to 10/rev.
The in-house rotor code includes different prescribed and free wake models. As the internal aerodynamic model is replaced by CFD aerodynamics during the coupling process the selection of such higher level downwash models is usually not beneficial. The advantage of a slightly better starting solution for the 0th trim is counterbalanced by a reduced robustness and execution speed. Hence the induced velocity distribution is computed using the Meijer-Drees analytical downwash model.

6. RESULTS

6.1. Trim Convergence

In Figure 8 the unsteady aerodynamic rotor loads are shown for the complete weak coupling process. Exemplarily the distribution is plotted for the weak coupling process between FLOWer and CAMRAD II. The evolution of unsteady rotor loads for the coupling between FLOWer and the in-house rotor code looks very similar.
In Figure 8 each re-trim is marked off with respect to the preceding trim by the line type change from solid to dash and vice versa. It can be clearly seen that the disturbance introduced by the update of the blade dynamic response decreases from each re-trim cycle to the next as the procedure converges towards the trimmed state. After four re-trims (five rotor revolutions) the calculation has reached the trimmed state with the required accuracy. Looking at Figure 8 one gets the impression that the mean value of the unsteady thrust is slightly below the prescribed objective. This is due to the fact the unsteady thrust does not feature a strictly sinusoidal shape due to additional 8/rev contributions. A computation of the mean value over a quarter of a rotor revolution reveals that the mean value of the unsteady thrust meets the prescribed trim objective with only 0.08% deviation.

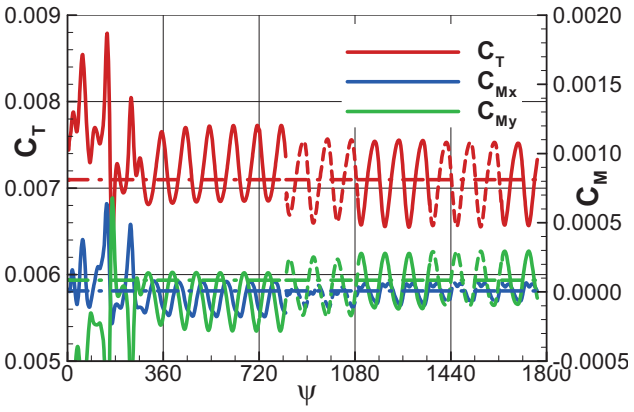

Figure 8: CFD rotor loads versus the coupling iterations

The corresponding development of the free controls is given in Figure 9. The evolution of the control angles for both the in-house rotor code and CAMRAD II are compared to the flight test values. The Figure shows that both the control angles predicted by CAMRAD II and the control angles predicted by the in-house code are in good agreement to the flight test values. Especially the longitudinal cyclic is in excellent agreement, indicating a correct mast moment capacity of the dynamic blade models. A difference between the codes is spotted for the collective pitch setting. The reason for this deviation will be addressed further below.

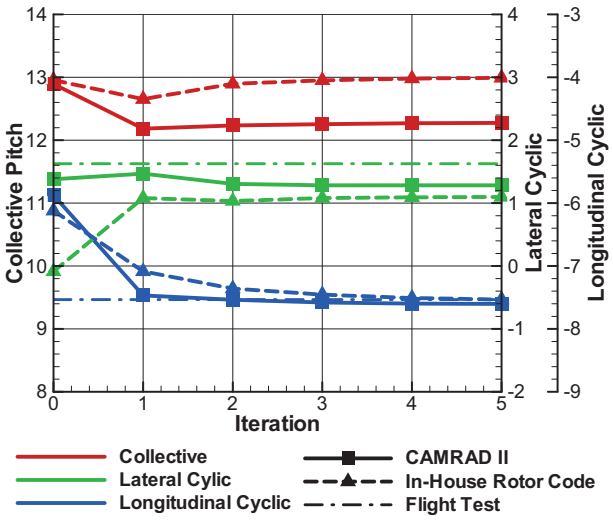

Figure 9: Trim evolution of rotor control angles

.

6.2. Rotor Performance

As already discussed in section 5.1 the measured engine power needs to be corrected for tail rotor power, auxiliary devices power and gearbox losses in order to obtain the net main rotor power. One has to emphasize that the error margin of the resulting power required can be in the range of a few percent, mainly because the power related to auxiliary devices and tail rotor was not measured. Hence the comparison with computational results has to be considered with reservation.

When looking at the computational results one can easily check for the conservativity of the coupled scheme by comparing the main rotor power consumption on CFD side and on comprehensive code side in almost converged state. In this case the comprehensive code aerodynamics should have been almost completely replaced by CFD aerodynamics and hence both values should be identical. Performing this comparison for CAMRAD II / FLOWer coupling the difference in power consumption is only 0.08%. This underlines the conservative implementation. The remaining small difference is due to the fact that the comprehensive code aerodynamics only cancels out completely if an exactly converged state of the coupled method could be reached. In reality the coupling is stopped as soon as the changes in the controls have fallen below some limit and hence some small difference in the aerodynamics on either side remains.
Naturally the line-loads based coupling does not feature the same level of conservativity. Here the deviation in rotor power is approximately 0.8% which is still acceptable. One has to emphasize that this is not a deficiency of the in-house rotor code but due to the realization of the coupling interface.

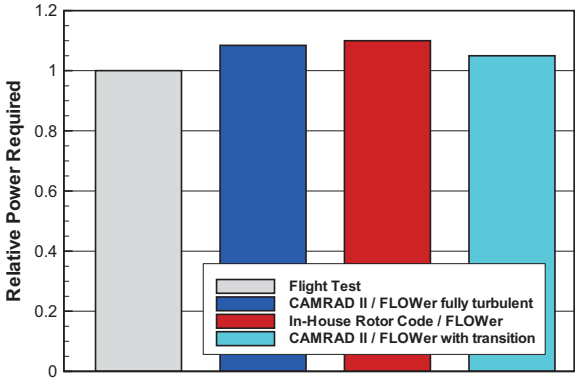

Figure 10: Relative rotor power required

The actual comparison of the predicted rotor power required to the value derived from flight test is provided in Figure 10. The coupled method overpredicts the power by roughly 8%. This comes as expected as the CFD computation is performed in fully turbulent manner. If transition was included, the laminar portion of the boundary layer would lead to a reduction in shear stress and hence to a reduced power requirement. Unfortunately transition models in the rotating frame are not yet state of the art and the helicopter community is lacking of reliable experimental transition data. It was decided to judge the influence of transition by a simple azimuth-angle *independent* transition prescription. The authors are

aware that this prescribed transition approach is an approximation but at least it gives a good estimate of the level of improvement to be expected from a more sophisticated transition prescription or transition modelling. Transition was prescribed at 10% chord on the upper side and at 60% chord on the lower side for the complete blade span. The result is also shown in Figure 10. It can be seen that the deviation from flight test is reduced to 4%, equivalent to a 50% reduction of the overestimation.

The result shows that transition is – among others – one of the key aspects for improvement of rotor performance prediction by CFD. However, as CFD claims to reproduce the flow by a full prediction capability, the ultimate goal is to model transition and not to prescribe it.

6.3. 3D Flow Field

The 3D flow field of the rotor has been analyzed from both the CFD solution and the CAMRAD II free-wake modelling. A comparison between the tip vortex trajectories of the two approaches is shown in Figure 11. The CFD vortex system has been computed using the well-known λ_2 vortex criterion of Jeong and Hussain [18]. An iso-surface at λ_2 = -0.001 was selected for visualization.

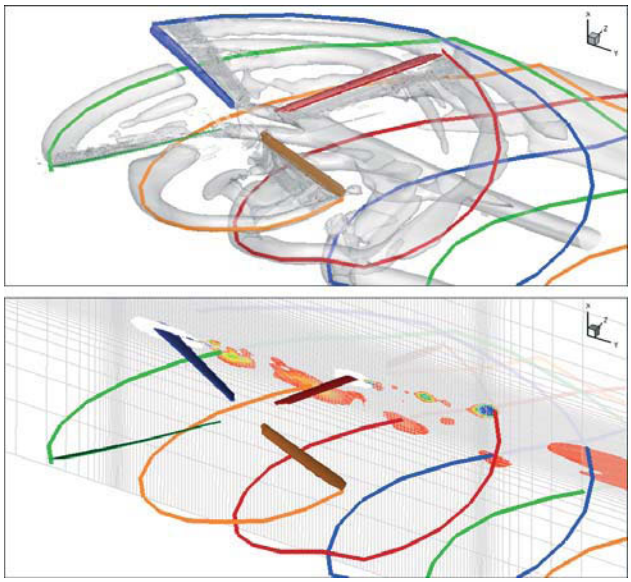

Figure 11: Comparison of CFD wake with CAMRAD II free-wake trajectories

The tip vortex trajectories obtained with the CAMRAD II baseline free-wake model have been superimposed to the CFD wake system. An isometric view of this comparison is provided in the top part of Figure 11. As the CFD Cartesian background mesh is comparatively coarse the CFD tip vortices dissipation and dispersion is rather high. Nevertheless the Figure illustrates that the free wake trajectories match generally quite well to the vortex cores of the CFD simulation.
The lower part of Figure 11 shows a similar representation but the illustration of the CFD wake is restricted to λ_2 contours in a longitudinal slice at r/R = 0.45 on the starboard side. One can see that the piercing points of the free-wake trajectories with the cutting plane coincide fairly well with the CFD vortex cores.
Note that the additional distinct vortex immediately behind the advancing rotor blade is not reproduced by the free-wake simulation. A cross-check with the top part of Figure 11 reveals that this vortex stems from the deflected trailing edge tab. As the tab is not separately treated by the baseline free-wake model its vortex wake is not directly reproduced.

The strength of the tab vortex can be estimated from the upper part of the Figure: The tip vortex shed from the blade indicated in green interacts with the tab vortex of the blue blade. As a consequence of this interaction the CFD trajectory of the resulting merged vortex differs from the Free-Wake trajectory (green line) in the second quadrant of the rotor disk.

6.4. Rotor Aeromechanics

The trailing edge tab does not only play an important role for the vortex wake system, as seen in the previous section, but its consideration is even more essential for the correct reproduction of the rotor aerodynamics and hence also the coupled aeromechanic behaviour.

The effect of the trailing edge tabs on the rotor aerodynamics is illustrated by Figures 12 and 13. Figure 12 shows radial distributions of C_nMa^2 and C_mMa^2 at ψ = 90° and ψ = 270°. One can easily spot the discontinuities in the distributions at the radial tab boundaries. While the effect on the sectional normal force is less pronounced, the deflected tab causes a massive disturbance in the sectional pitching moment distribution, especially on the advancing side.

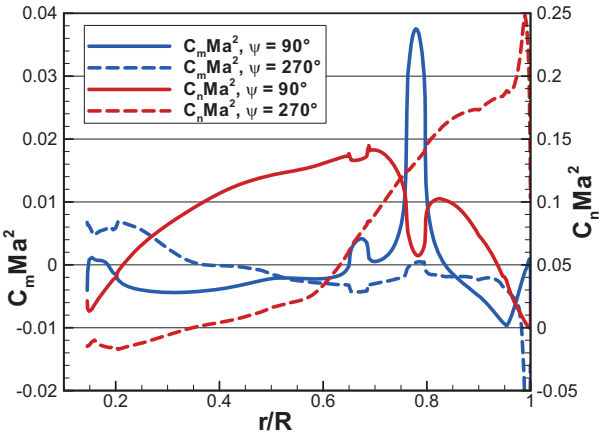

Figure 12: C_nMa^2 and C_mMa^2 distributions from coupled CAMRAD II / FLOWer result

The effect on the pitching moment is caused by the pressure distribution in the tab region. Figure 13 shows the sectional pressure distribution of the advancing blade for a radial station centered in the spanwise range of the deflected tab (r/R = 0.77). The kink in the contour leads to a suction peak on the lower side and a higher pressure region on the upper side. The corresponding down force leads to the pitch-up moment around the quarter chord point seen in Figure 12.

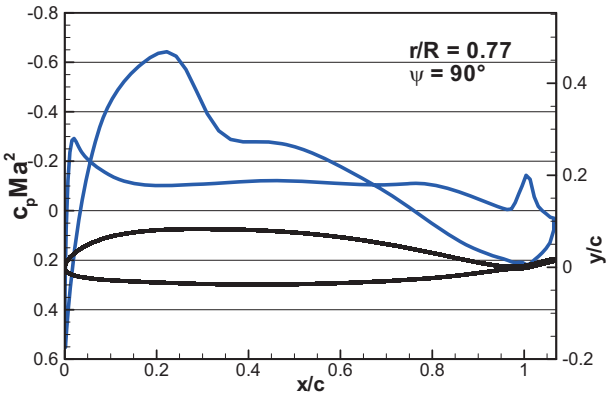

Figure 13: Sectional pressure distribution from coupled CAMRAD II / FLOWer result

The rotor dynamic behaviour is shown in Figures 14 and 15. Figure 14 illustrates the influence of the CFD aerodynamics on the blade dynamic response, exemplarily plotted for the 0th and 1st coupling iterations between CAMRAD II and FLOWer. The blade surfaces shown in blue correspond to the initial (0th) CAMRAD II solution obtained without CFD. The consideration of CFD aerodynamics during the 1st re-trim process leads to a modified dynamic response, illustrated by the blade surfaces in yellow. The overall characteristics of the blade dynamics look similar but a closer look reveals that the CFD aerodynamics leads to changes in both the modal contributions and their amplitudes.

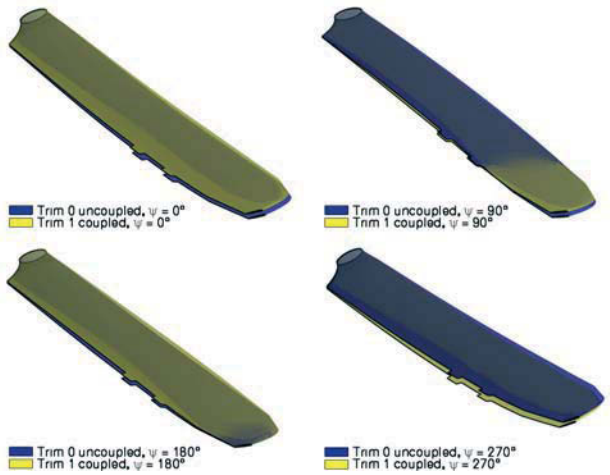

Figure 14: Comparison between CAMRAD II blade dynamics of trim 0 and trim 1

Figure 15 shows the blade pitch characteristics after convergence of the coupling with CFD. Both the results of CAMRAD II / FLOWer and in-house rotor code / FLOWer coupling are shown. Note that three different portions of the pitch are shown: Firstly the overall pitch attitude at the blade tip (solid line), secondly the control input, i.e. the blade pitch at the pitch hinge (thin dash-dotted line), and thirdly the difference between the two angles, corresponding to the elastic blade twist (dashed line).

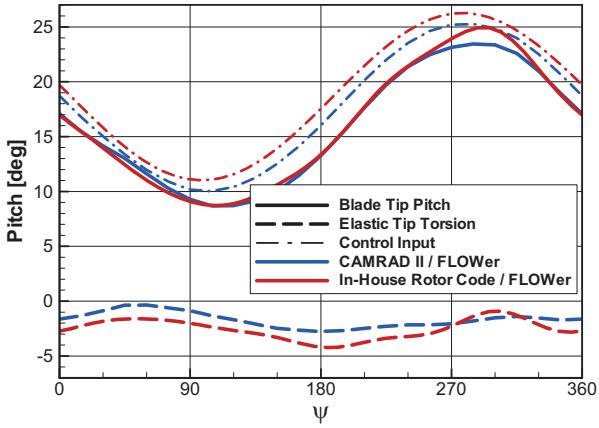

Figure 15: Comparison of CAMRAD II and in-house rotor code blade pitch and torsion characteristics

It can easily be seen that the overall blade tip pitch distribution of both codes is very similar. This does not come as a surprise, as the rotor has been trimmed towards prescribed objectives.
However the control input at the pitch hinge is different between the codes. While the azimuthal variation is almost identical (corresponding to almost identical values of the two cyclic pitch control inputs, see Figure 9), the mean value shows a deviation of roughly one degree. This is in line with the findings from Figure 9.
The reason is the elastic torsion behaviour of the blade (dashed line). The elastic tip torsion predicted by the in-house rotor code is roughly one degree higher (more nose-down) than the one predicted by CAMRAD II. This needs to be compensated by a higher collective pitch setting in order to end up with the same rotor thrust. The reason for this discrepancy needs to be investigated in more detail. Another difference in the prediction of the torsional response is spotted around ψ = 300°. The in-house rotor code computes a nose-up torsion peak, or to be more precisely, a reduction of nose-down elastic torsion. This peak remains visible in the overall blade tip pitch attitude (solid line).

6.5. Blade Loads

This section presents the blade loads results obtained from the CAMRAD II / FLOWer and in-house rotor code / FLOWer coupled predictions for the sensor locations specified in section 5.1. In addition a comparison between the coupled predictions and

different CAMRAD II Free-Wake results is presented for the flap moment sensor MB3410. We restrict this comparison to one of the sensors due to the limited space available.

The following Figures 16 to 21 compare the coupled results to flight test data. The flight test data were recorded over 72 subsequent rotor revolutions equivalent to roughly 11s of recording time. The scatter of the bunch of grey lines representing the recorded 72 revolutions is hence an indicator for the steadiness of the flight state. The Figures show that the distributions reproduce very well for all of the sensors.
The black line represents the mean value over all rotor revolutions. Note that a filter was used during data acquisition. Its phase delay was compensated leading to a slight shift of the flight test reference relative to the centreline of the line bunch.
The Figures compare the azimuthal variation only, the mean values have been removed. The mean value is subject to the calibration of the strain gages (calibration in non-rotating state including blade weight) and hence different to the models. For this paper priority is given on the reproduction of Peak-to-Peak amplitude and frequency content which are more essential for assessing the maturity and the potential benefits of CFD plus coupling.

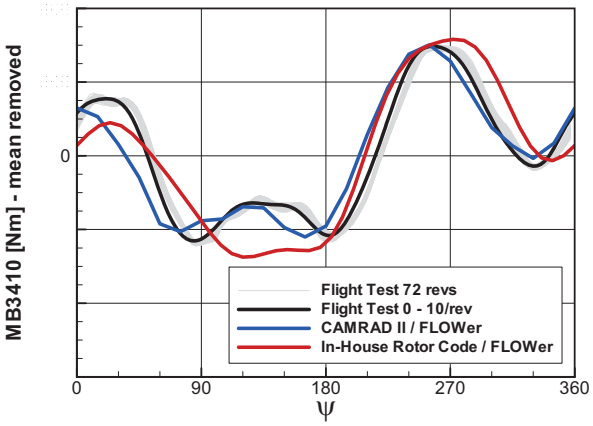

Figure 18: Flap moment at r = 3.410m

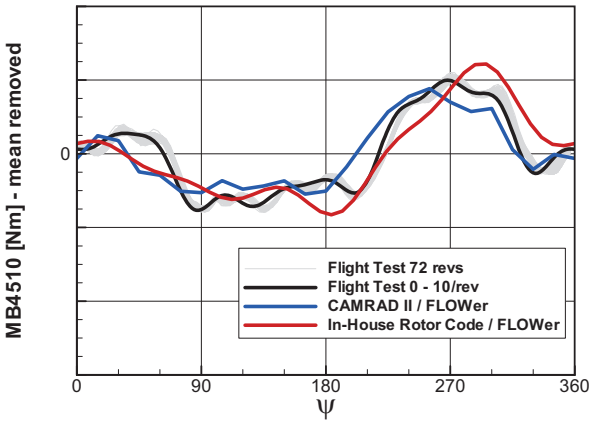

Figure 19: Flap moment at r = 4.510m

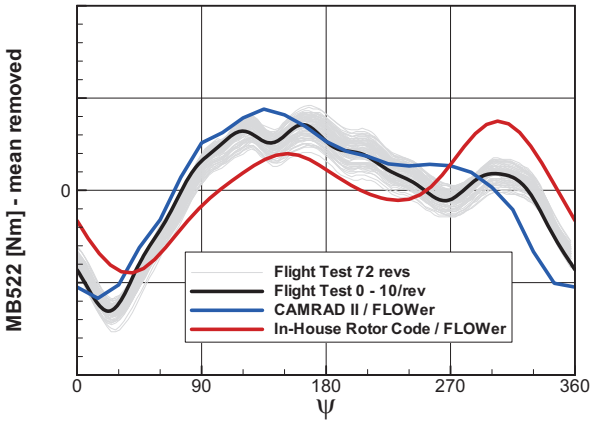

Figure 16: Flap moment at r = 0.522m

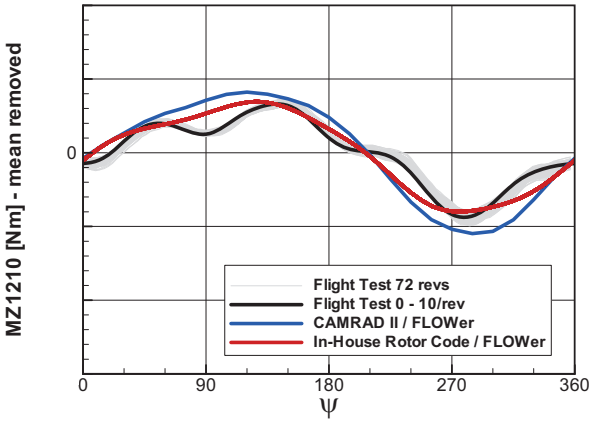

Figure 20: Lag moment at r = 1.210m

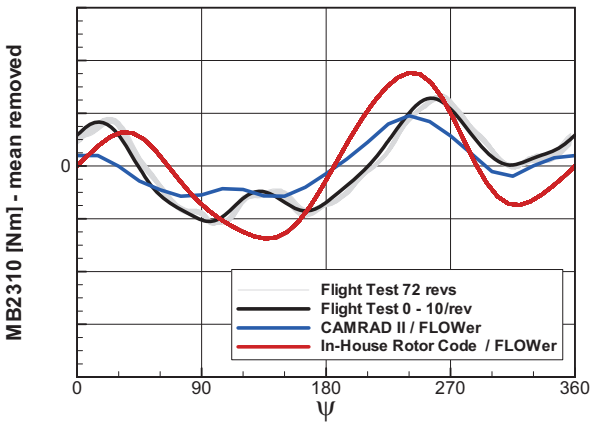

Figure 17: Flap moment at r = 2.310m

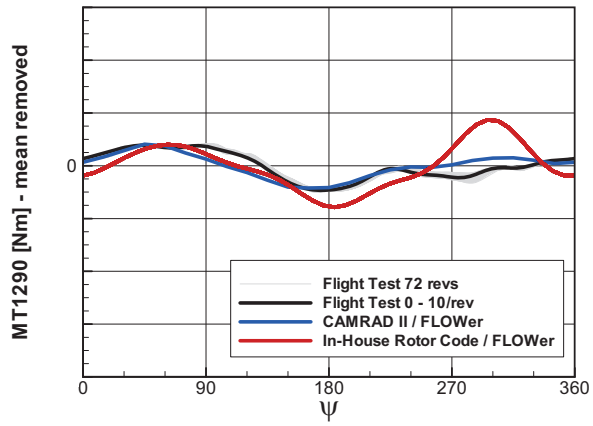

Figure 21: Torsion moment at r = 1.290m

As a general statement one can note that the overall agreement is good for all sensors. Especially the outboard flap moment is excellently reproduced. The lag moment distribution at r = 1.21m reveals a 4/rev component which is not reproduced by the numerical simulation. The authors suppose that this 4/rev contribution is due to the interaction with the drive train. A drive train model was neither incorporated into the CAMRAD II nor into the in-house rotor code dynamic model.
Comparing the two comprehensive code predictions the CAMRAD II result is in better agreement to the flight test measurements. This does not come as a real surprise as the CAMRAD II dynamic model is assessed to be more realistic e.g. in the view of the implemented flap absorbers and the adequate consideration of control flexibility missing in the numerical model of the other code.

The only remarkable inconsistency arises in the prediction of the torsion moment at r = 1.29m where the in-house rotor code predicts a peak around ψ = 300°. This peak is clearly linked to the elastic torsion peak spotted in Figure 15. This behaviour needs further investigation.

Figure 22 and Figure 23 show a comparison between the coupled CAMRAD II / FLOWer result and CAMRAD II results using various Free-Wake models. The comparison is performed for the flap bending moment at r = 3.410m.

In Figure 22 three different result sets for conventional roll-up Free-Wake models are plotted versus flight tests and CFD based results. The applied wake models differ by the wake configuration for the far wake: The first model is based on the maximum circulation magnitude for the tip vortex and the second one on the outboard circulation magnitude while the third one considers two circulation peaks using a dual peak model which is able to adequately take into account negative blade tip loading e.g. experienced in fast forward flight. The differences between the models are especially visible at an azimuth angle starting at around 90° where a negative tip loading of the blade exists. It should be noted in addition that no tuning of the wake models was performed.
In Figure 23 three different result sets are presented for multiple trailer wake models. Multiple trailer wake models differ from conventional roll-up models in CAMRAD II by considering the trailed vorticity from each panel. Results are compared for the cases without consolidation and with consolidation of the trailed vortex lines. Regarding consolidation, two different schemes are available labelled entrainment and compression. Again significant differences between the models are visible in the azimuth range of 90° to 180°.

Summarizing one can say that none of the Free-Wake models reaches the prediction level of the coupled CAMRAD II / FLOWer calculation for this test case.

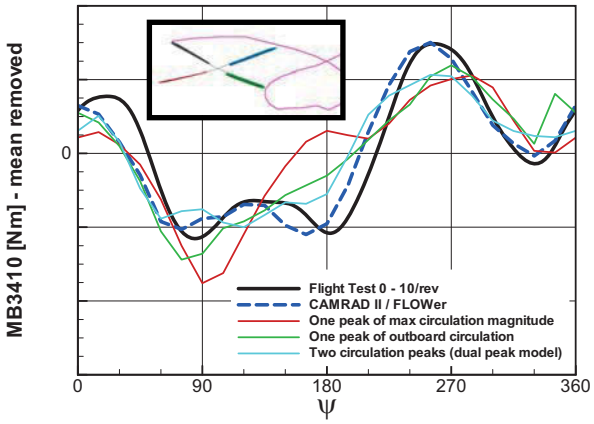

Figure 22: Flap moment at r = 3.410m, CAMRAD II Free-Wake (conv. roll-up models)

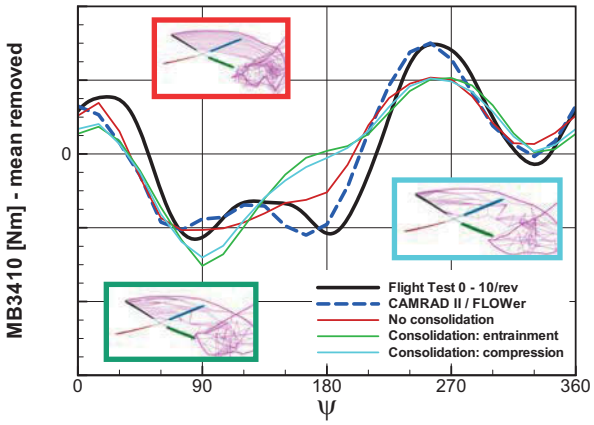

Figure 23: Flap moment at r = 3.410m, CAMRAD II Free-Wake (multiple trailer models)

6.6. Complete Helicopter Simulation

The continuous further development of CFD and increasing computational resources allow for the CFD simulation of a complete helicopter. As a consequence the extension of the coupling and trim functionality towards the trimmed CFD simulation of the complete helicopter is obvious. The full CFD modeling of the helicopter will allow for a significant improvement in the reproduction of local and interactional aerodynamics. This should lead both to an improved helicopter performance prediction and to a further improvement in loads prediction and reproduction.

For the short and mid term future the CFD simulation of the complete helicopter represents a key research topic but not yet an industrial process. For this reason the related development activities are performed in close cooperation with the Institute of Aerodynamics and Gas Dynamics of University of

Stuttgart. IAG's activities will focus mainly on a free-flight trim capability between FLOWer and Eurocopter's comprehensive code. The EC145 helicopter has been selected as the reference configuration. The CFD grid system of the complete helicopter configuration has been set up by ECD and is presented in Figure 24. It includes the main rotor, the two-bladed tail rotor and the EC145 fuselage including landing skids. Note that in this first stage the rotor head is not included in the CFD grid system. Instead, it will be modeled by an advanced rotor head model within the comprehensive code. The overall grid system consists of 11 block structures, 302 blocks and roughly 25 million grid cells.

Figure 24: Surface mesh of EC145 complete helicopter grid system

As a first application of the grid system we decided to perform a complete helicopter simulation prescribing the last rotor trim state (re-trim 4) of the coupled CAMRAD II / FLOWer isolated rotor trim presented in the previous sections. Note that the helicopter used for the flight test was the BK117. Hence the fuselage used in the CFD simulation does not perfectly match the actual configuration. Nevertheless it is justified to judge the blockage effect of the fuselage on the rotor trim state.

Figure 25 shows the Delta in the rotor disk thrust distribution obtained from subtracting the isolated rotor thrust distribution from the distribution of the complete helicopter computation. It is again emphasized that the "frozen" rotor dynamics of the last isolated rotor trim was prescribed for the complete helicopter configuration. As a consequence of that the rotor is not in a trimmed state anymore.

Figure 25 shows that the blockage effect of the fuselage leads to increased thrust in the front part of the disk and to thrust reduction in the rear part. This additional 1/rev dominated thrust variation should lead to a flap response with a phase delay of roughly 80°, i.e. flapping upwards at ψ = 260° and flapping downwards at ψ = 80°. This should be related to a roll right moment. One would expect a correction of the lateral cyclic towards a higher value, corresponding to a higher pitch around ψ = 0° and a lower pitch ψ = 180°. This is confirmed by the CAMRAD II control angles of re-trim 5 using the complete helicopter CFD rotor loads which were computed from the rotor dynamics of the isolated rotor trim 4. The control angles are provided in Table 3.

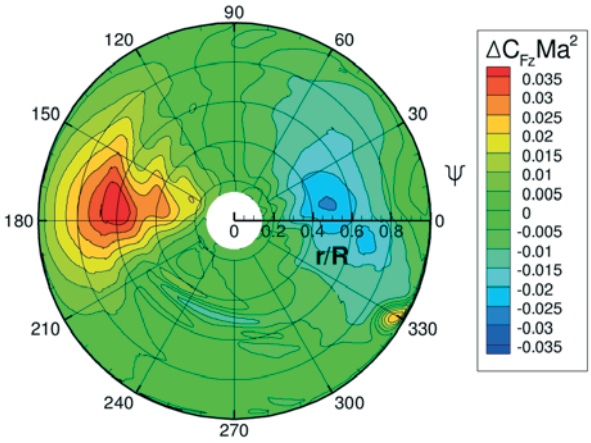

Figure 25: Delta in thrust distribution on rotor disk, complete helicopter minus isolated rotor

Trim iter. 5	Collective	Long. Cyclic	Lateral Cyclic
Isolated rotor	12.274	-7.603	1.282
Complete H/C	12.494	-7.994	1.679

Table 3: Control angle changes due to fuselage interference

As expected the lateral cyclic pitch angle is increased by about 0.4°. At the same time the longitudinal cyclic pitch angle was further reduced by about 0.4° and the collective pitch was slightly increased. A comparison with Figure 9 reveals that the lateral control input tends to further approach the flight test value while the agreement of the longitudinal control input with the flight test value is slightly reduced. A final conclusion can however only be drawn after another re-trim, based on updated CFD rotor loading, has been performed.

Finally Figure 26 gives an impression of the 3D flow field of the complete helicopter configuration. The vortex system has been visualized using the λ_2 criterion as already described in section 6.3. The Figure clearly shows the high complexity of the flow field which is dominated by interference effects between main rotor wake, fuselage wake and tail rotor wake. This underlines the potential for further improvement of performance and blade loads prediction by consideration of further helicopter components in the CFD part of the simulation.

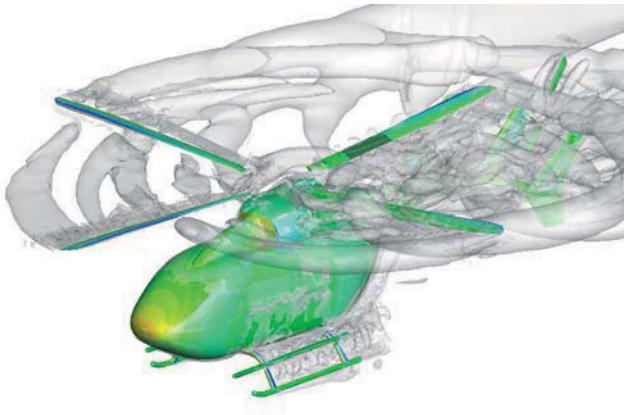

Figure 26: 3D flow field of complete helicopter configuration

7. CONCLUSION AND OUTLOOK

We have presented recent activities in rotor aeroelastic computations in industry. The aerodynamic modelling was mainly carried out by CFD, while the structural modelling and the trim task were performed by two different comprehensive codes. Additionally a comparison of the coupled CFD predictions to Free-Wake analysis was performed.
The aeroelastic CFD analysis was performed using the weak coupling methodology. A weak coupling interface between FLOWer and CAMRAD II has been newly developed and integrated into an industrial framework.

The results obtained for the computed isolated rotor test case are generally very promising and in good agreement to flight test data. The experimental cyclic rotor controls are excellently reproduced by the coupled prediction and a clear improvement in comparison to the initial comprehensive code values is achieved by the consideration of CFD.

The incorporation of CFD has also lead to a significant improvement in blade loads reproduction. The coupled CFD blade load predictions are generally in good agreement to flight test values. Despite the simpler dynamic blade model of the in-house rotor code the loads reproduction is not far below the CAMRAD II results. An exception is the blade torsion prediction which needs to be further investigated.
The lag bending moment comparison revealed that the 4/rev component is not reproduced probably being related to a missing drive train model in the dynamic model.

Concerning rotor performance CFD tends to overestimate the required rotor power. It was shown that the incorporation of transition leads to a 50% reduction of the relative error and leads to a performance overprediction of about 4%.

Future activities will include further improvements in both the aerodynamic and dynamic model. A drive train model will be included into the CAMRAD II model in order to improve the prediction of the lag bending. The dynamic blade model of the in-house rotor code will be upgraded in order to further improve the loads prediction. This task is performed in close cooperation with ONERA.

The improvement of the aerodynamic modelling focuses on the consideration of further helicopter components in the CFD simulation. This will go in line with an upgrade of the coupling interface in order to establish a complete helicopter free flight trim. The corresponding developments are performed in close cooperation with IAG. We expect that the improved reproduction of interactional aerodynamics will lead both to an improved helicopter performance prediction and to a further improvement in loads prediction and reproduction.

ACKNOWLEDGEMENTS

The authors would like to thank the German ministry of Economy and Technology (BMWi) for its funding in the framework of SHANEL-L (grant 20A0603C).

REFERENCES

[1] Costes, M., Raddatz, J., Borie, S., D'Alascio, A., Embacher, M.: *"Advanced Rotorcraft Aeromechanics Studies in the French-German SHANEL Project"*, Proceedings of the 35th European Rotorcraft Forum, Hamburg, Germany, September 2009.

[2] Kroll, N., Eisfeld, B. and Bleecke, H.M., "*The Navier-Stokes Code FLOWer"*, Volume 71 of Notes on Numerical Fluid Mechanics, pages 58-71. Vieweg, Braunschweig, 1999.

[3] Johnson, W.: *"Technology Drivers in the Development of CAMRAD II"*, AHS Aeromechanics Specialists' Conference, San Francicso, CA, 1994.

[4] Kroll, N., Rossow, C.-C., Becker, K., Thiele, F.: *"The MEGAFLOW Project"*, Aerospace Science and Technology, No. 4, 2000, pp. 223-237.

[5] Costes, M., Pahlke, K., D'Alascio, A., Castellin, C., Altmikus, A.: *"Overview of results obtained during the 6-year French-German CHANCE project"*, AHS 61st Annual Forum, Grapevine, TX, June 2005.

[6] Jameson, A., Schmidt, W. and Turkel, E.: *"Numerical Solutions of the Euler Equations by Finite Volume Methods Using Runge-Kutta Time-Stepping Schemes"*, AIAA-Paper 81-1259, 1981.

[7] Jameson, A.: *"Time Dependent Calculation Using Multigrid, With Applications to Unsteady Flows Past Airfoils and Wings"*, AIAA-Paper 91-1596, 1991.

[8] Schwarz, Th.: *"The Overlapping Grid Technique for the Time-Accurate Simulation of Rotorcraft Flows"*, Proceedings of the 31st European Rotorcraft Forum, Florence, Italy, September 2005.

[9] Dietz, M.: *„Simulation der Umströmung von Hubschrauberkonfigurationen unter Berücksichtigung von Strömungs-Struktur-Kopplung und Trimmung"*, PhD Thesis, Verlag Dr. Hut, ISBN 978-3-89963-942-1, 2009.

[10] Johnson, W.: *"A General Free Wake Geometry Calculation for Wings and Rotors"*, AHS 51st Annual Forum, Fort Worth, TX, 1995.

[11] Johnson, W.: *"Rotorcraft Dynamics Models for a Comprehensive Analysis"*, AHS 54th Annual Forum, Washington, DC, 1998.

[12] Altmikus, A. Wagner, S., Beaumier, P., Servera, G.: *"A Comparison: Weak versus Strong Modular Coupling for Trimmed Aeroelastic Rotor Simulations"*, American Helicopter Society 58th Annual Forum, June 2002.

[13] Servera, G., Beaumier, P., Costes, M.: *"A weak coupling method between a dynamics code and the 3D unsteady Euler code WAVES"*, Proceedings of the 26th European Rotorcraft Forum, The Hague, The Netherlands, September 2000.

[14] Pahlke, K., Van der Wall, B., *"Calculation of Multibladed Rotors in High-Speed Forward Flight with weak Fluid-Structure-Coupling"*, Proceedings of the 27th European Rotorcraft Forum, Moscow, Russia, September 2001.

[15] Potsdam, M., Yeo, H., Johnson, W.: *"Rotor Airloads Prediction Using Loose Aerodynamic/Structural Coupling"*, AHS 60th Annual Forum, Baltimore, MD, June 2004.

[16] Dietz, M., Altmikus, A., Krämer, E., Wagner, S.: *„Weak Coupling for Active Advanced Rotors"*, Proceedings of the 31st European Rotorcraft Forum, Florence, Italy, September 2005.

[17] Johnson, W.: *"Calculation of the aerodynamic behaviour of the tilt rotor aeroacoustic model (TRAM) in the DNW"*, 57th AHS Annual Forum, Washington DC, 2001.

[18] Jeong, J., Hussain, F., *"On the Identification of a Vortex"*, Journal of Fluid Mechanics, Vol. 285, pp. 69-94, 1995.